overcome the pressure offered by the air present within the HOF. The elasticity of the air thus determine a pressure variable during the HOF dipping and it represents a good exemplification of the effect of the pressure on the deposition which can be otherwise properly controlled.

4. CONCLUSIONS

In summary, the far field characterizations reveal the success of the SWCNTs deposition demonstrating the partial filling of the nanotubes within HOFs. Also, the obtained results demonstrate that the main effect of SWCNTs filling is the significant modification of the guiding properties and thus of the local PBG at the termination of the HOF. Also, by using the LB deposition method, we demonstrate how by acting on the process parameters and especially on monolayers number and pressure conditioning at the free termination, it would be possible to optimize and tailor the SWCNTs filling enabling the local control of the HOF PBG. The proper modification of the HOF PBG features, by filling (also selectively) the HOF holes with SWCNTs, can supply, in fact, to the final device advanced functionalities and can be properly exploited to develop high performances sensors based on PBG modification as well as multimaterial and multifunctional fibers.

REFERENCES

1. A.F. Abouraddy, M. Bayindir, G. Benoit, S.D. Hart, K. Kuriki, N. Orf, O. Shapira, F. Sorin, B. Temelkuran, and Y. Fink, Towards multimaterial multifunctional fibres that see, hear, sense and communicate, Nature 6 (2007), 336–347.
2. J.C. Knight, Photonic crystal fibres, Nature 424 (2003), 847–851.
3. P. Domachuk, H.C. Nguyen, B.J. Eggleton, M. Straub, and M. Gu, Microfluidic tunable photonic band-gap device, Appl Phys Lett 84 (2004), 1838–1840.
4. T.T. Larsen, A. Bjarklev, D.S. Hermann, and J. Broeng, Optical devices based on liquid crystal photonic bandgap fibres, Opt Exp 11 (2003), 2589–2596.
5. Y. Huang, Y. Xu, and A. Yariv, Fabrication of functional microstructured optical fibers through a selective-filling technique, Appl Phys Lett 85 (2004), 5182–5184.
6. F. Benabid, F. Couny, J.C. Knight, et al., Compact, stable and efficient all-fibre gas cells using hollow-core photonic crystal fibres, Nature 434 (2005), 488–491.
7. V. Matejec, J. Mrázek, M. Hayer, I. Kašík, P. Peterka, J. Kanka, et. al. Microstructure fibers for gas detection, Mater Sci Eng C 26 (2006), 317–321.
8. M.S. Dresselhaus, G. Dresselhaus, and Ph. Avouris, Carbon nanotubes: synthesis, structure, properties, and applications, In: Topics in applied physics, Vol. 80, Springer, Berlin, 2001.
9. M. Penza, G. Cassano, P. Aversa, A. Cusano, A. Cutolo, M. Giordano, and L. Nicolais, Carbon nanotube acoustic and optical sensors for volatile organic compound detection, Nanotechnology 16 (2005), 2536–2547.
10. M. Penza, G. Cassano, P. Aversa, F. Antolini, A. Cusano, A. Cutolo, M. Giordano, and L. Nicolais, Alcohol detection using carbon nanotubes acoustic and optical sensors, Appl Phys Lett 85 (2004), 2379–2381.
11. A. Cusano, M. Pisco, M. Consales, A. Cutolo, M. Giordano, M. Penza, P. Aversa, L. Capodieci, and S. Campopiano, Novel opto-chemical sensors based on hollow fibers and single walled carbon nanotubes, IEEE Photon Technol Lett 18 (2006), 2431–2433.
12. M. Pisco, M. Consales, A. Cutolo, M. Penza, P. Aversa, and A. Cusano, Hollow fibers integrated with single walled carbon nanotubes: bandgap modification and chemical sensing capability, Sensors Actuator B: Chem 129 (2008), 163–170.
13. K. Nielsen, D. Noordegraaf, T. Sørensen, A. Bjarklev, and T. P Hansen, Selective filling of photonic crystal fibres, J Opt A: Pure Appl Opt 7 (2005), L13–L20.

BANDGAP PROPERTIES OF LOW-INDEX CONTRAST APERIODICALLY ORDERED PHOTONIC QUASICRYSTALS

Gianluigi Zito,[1] T. Priya Rose,[2] Emiliano Di Gennaro,[1] Antonello Andreone,[2] Enrico Santamato,[1] and Giancarlo Abbate[2]

[1] CNISM and Department of Physics, University of Naples Federico II, Napoli, Italy; Corresponding author: gianluigi.zito@na.infn.it

[2] CNR-INFM Coherentia and Department of Physics, University of Naples Federico II, Napoli, Italy

Received 22 May 2009

ABSTRACT: *We numerically analyze, using Finite Difference Time Domain simulations, the bandgap properties of photonic quasicrystals with a low-index contrast. We compared 8-, 10-, and 12-fold symmetry aperiodically ordered lattices with different spatial tiling. Our results show that tiling design, more than symmetry, determines the transmission properties of these structures.* © 2009 Wiley Periodicals, Inc. Microwave Opt Technol Lett 51: 2732–2737, 2009; Published online in Wiley InterScience (www.interscience.wiley.com). DOI 10.1002/mop.24724

Key words: *band-gap materials; photonic quasicrystals; finite difference method*

1. INTRODUCTION

Quasicrystals are structures exhibiting long-range aperiodic order and rotational symmetry [1, 2]. A quasi-lattice can fill up the entire space to form an infinite structure with forbidden rotational symmetry for periodic crystals. The unit cells overlap each other in a complex manner repeating along the symmetry axis [1]. Although lacking an overall absolute translational symmetry, this local overlapping periodicity acts as a superimposed Bragg grating and gives rise to multiple forbidden photonic band-gap (PBG) frequencies. Photonic QuasiCrystals (PhQCs) may exhibit PBG [3, 4] that are more isotropic than in conventional photonic crystals, permitting the existence of forbidden frequency ranges even in materials possessing very low dielectric contrast. The photonic quasi-lattices are artificial dielectric inhomogeneous media, where scattering centers are usually located in the vertices of the tiles [5]. The quasiperiodic order gives rise to many nonequivalent defect sites, increasing the flexibility of these materials for different photonic applications and leading to interesting properties for confining and guiding electromagnetic energy [6, 7]. Superlensing effect, directive emission, and mode confinement [8–11] are examples of the quasicrystal features that have recently attracted tremendous interest because of their potential impact in optical components.

Typically, a complete PBG in photonic crystals can be achieved by using materials with a refractive index contrast substantially higher than zero. Recent studies on quasicrystals with 8-fold (octagonal point group) [3], 10-fold (decagonal), and 12-fold (dodecagonal) [8] rotational symmetries have shown that, in general, most of the PhQCs have wide complete bandgaps even for low-threshold values of the refractive index contrast. This characteristic entails the possibility of using a flexible and versatile low-cost technology combined with holographic or lithographic fabrication techniques able to realize both large-area and high quality structures in novel soft matter-based and silicon-based devices.

Recently, holographic techniques based on interferential schemes have been widely used to fabricate PhQCs with high rotational symmetries [12–17]. The light distribution obtained from the interference of two or many coherent light beams is transferred to a photosensitive medium producing the desired

quasiperiodic dielectric modulation by single or multiple exposure process. The scattering centers (typically, rods in a binary pattern) of the quasi-lattice correspond to the maxima positions of the light distribution resulting from the *N*-beam interference. The rotational symmetry is determined by the number of beams, whereas the particular tiling pattern of the structure depends on the light intensity, time exposure, and on the delicate balance among direction, polarization, amplitude, and phase of the beams [15]. By controlling the relative phase delay among the interfering beams, for instance, different geometries in the tiling of the dielectric medium are achievable [16].

Instead, by using direct writing techniques like the electron-beam or single laser beam lithography [18] the spatial tiling of the quasi-lattice can be determined point-by-point. In these cases, usually, the quasiperiodic tiling is previously determined by geometric rules or inflation algorithms. In the case of the octagonal Ammann-Beenker tiling [19, 20], the unit cells consist of "squares" and "rhombuses" of equal side length. Analogously, the Penrose aperiodic tiling may be realized with several approaches. We consider the Penrose tiling consisting of "fat and thin rhombuses," which shows a 10-fold rotational symmetry. Both resulting quasicrystals have fivefold rotational and mirror symmetry corresponding to a decagonal (10-fold) point group symmetry. Hence, we will refer to the Penrose "rhombus" pattern as decagonal. With regard to the PhQC of 12-fold rotational symmetry, we consider a dodecagonal tiling consisting of "squares" and "triangles" given by Stampfli inflation rule [11].

Although the rotational symmetry of the structure can be of the same order, the quasiperiodic lattices generated by using either interferential methods or geometric rules can exhibit a completely different geometry.

In this work, we numerically analyze using Finite Difference Time Domain (FDTD) simulations the transmittance spectra of 8-, 10-, and 12-fold quasicrystal structures. For each fixed rotational symmetry, two different quasiperiodic tilings are considered and compared.

2. QUASICRYSTAL DESIGN AND SIMULATIONS

Many different types of quasiperiodic structures have been proposed and studied in literature. In this article, we compare two different tiling patterns of two-dimensional (2D) symmetric quasi-lattices with 8-, 10-, and 12-fold point groups. For each symmetry, the two geometries were determined (a) using a geometric or inflation rule, and (b) assuming a multiple-beam interference process. Let us call geometric patterns the formers ones and label it with (A), and interferential patterns the latter ones, indicated by (B).

Holographic lithography permits to record large-area PhQCs in many kinds of photosensitive hard and soft materials, hence it represents an important fabrication technique largely used to realize high-quality quasiperiodic structures. The writing pattern of light is usually obtained as multiple-beam interference and, consequently, the resulting spatial pattern of the dielectric modulation is different from the quasicrystal patterns achievable from inflation tiling. In a typical experimental situation of *N*-beam interference [12, 16], the irradiance profile $I(\mathbf{r})$ achievable according to the relation

$$I(\mathbf{r}) = \sum_{m=I}^{N}\sum_{n=I}^{N} A_m A_n^* \exp[i(\mathbf{k}_m - \mathbf{k}_n)\cdot\mathbf{r} + i(\varphi_m - \varphi_n)], \qquad (1)$$

gives the quasiperiodic spatial distributions of the intensity maxima. Here A_m, $\mathbf{k}_m$, f_m, are the amplitudes, the wave vectors, and the initial phases of the interfering beams, respectively. The wave vectors $\mathbf{k}_m$ of the beams, for $m = (1, \ldots, N)$, are oriented, according to the relation

$$\mathbf{k}_m = \frac{2\pi n}{\lambda}\left(\sin\left(\frac{2\pi m}{N}\right)\sin\theta, \cos\left(\frac{2\pi m}{N}\right)\sin\theta, \cos\theta\right), \qquad (2)$$

at an angle θ with respect to the longitudinal direction along z-axis and are equally distributed along the transverse (x, y)-plane. n is the average refractive index of the medium and λ is the common wavelength of the beams. Usually, the beams are supposed to have the same linear polarization. Their number N is related to the rotational symmetry of the quasicrystal [17]. By changing the phase delay between the beams, different patterns having the same symmetry can be realized [16, 21]. The filling factor, defined as the ratio between the area of n_H (high-refractive index) regions and total area, depends on the threshold level of the photosensitive material and the exposure time and intensity. Typically, the maxima positions of the light pattern correspond to the high dielectric regions, which can be usually approximated with a structure of homogenous dielectric rods embedded in a host medium of different index.

Figure 1 shows the detail of the six different structures that were analyzed, in which the number of dielectric elements was held fixed to 900. The eightfold geometric structure octagonal (A) simulated and shown in Figure 1(a) consists of dielectric rods (high-index n_H medium) in air (low-index n_L medium) located at the vertices of the Ammann-Beenker tiling of space, that is the positions of the cylinders of radius r are coincident with the vertices of "squares" and "45° rhombuses" with sides of equal length. Recently, it was theoretically found that octagonal (A) pattern presents a complete PBG with a very low-threshold value for the refractive index contrast, suggesting the possibility to realize optoelectronic devices based on this tiling pattern in silica or even in soft materials like polymer [20]. In Figure 1(b), the eightfold interferential pattern is shown, calculated for $N = 8$ from Eqs. (1) and (2). The structure was obtained imposing a particular phase delay between the beams, that is the phases were periodically shifted by $\pi/2$ so that $\varphi_1 = \varphi_5 = 0$, $\varphi_2 = \varphi_4 = \varphi_6 = \varphi_8 = \pi/2$, and $\varphi_3 = \varphi_7 = \pi$. The pattern was obtained by positioning circular rods of radius r (top view in Fig. 1) in the maxima of the continuous irradiance distribution $I(\mathbf{r})$ resulting from Eq. (1) [22]. The quasicrystal lattice is, therefore, determined without calculating a particular tiling of the plane. Nevertheless, the spatial tiling can be easily derived after having generated the structure. The patterns depicted in Figures 1(a) and 1(b) are clearly different. Although they possess the same rotational symmetry, the tiling originating the pattern provides a different assembly of the dielectric elements. The particular interferential pattern of Figure 1(b), octagonal (B), was studied in a preliminary work [22].

The patterns shown in Figures 1(c) and 1(d) are 10-fold quasicrystals obtained from the geometric Penrose tiling with rhombic cells [23] of equal side length [decagonal (A)], and supposing a 10-beam interference [decagonal (B)], respectively. In Figures 1(e) and 1(f), the dodecagonal (A) and (B) patterns obtained from inflation algorithm and 12-beam interference, respectively, are shown. In particular, dodecagonal (A) is a 12-fold quasicrystal formed with triangle-square tiling by a recursive algorithm and scaled up by an inflation factor, which was found to induce a photonic bandgap even in host medium with low-threshold index like glass [4]. Multiple-beam patterns of both 10- and 12-fold symmetry have been calculated from Eqs. (1) and (2) supposing a typical holographic process of fabrication in which the beams have

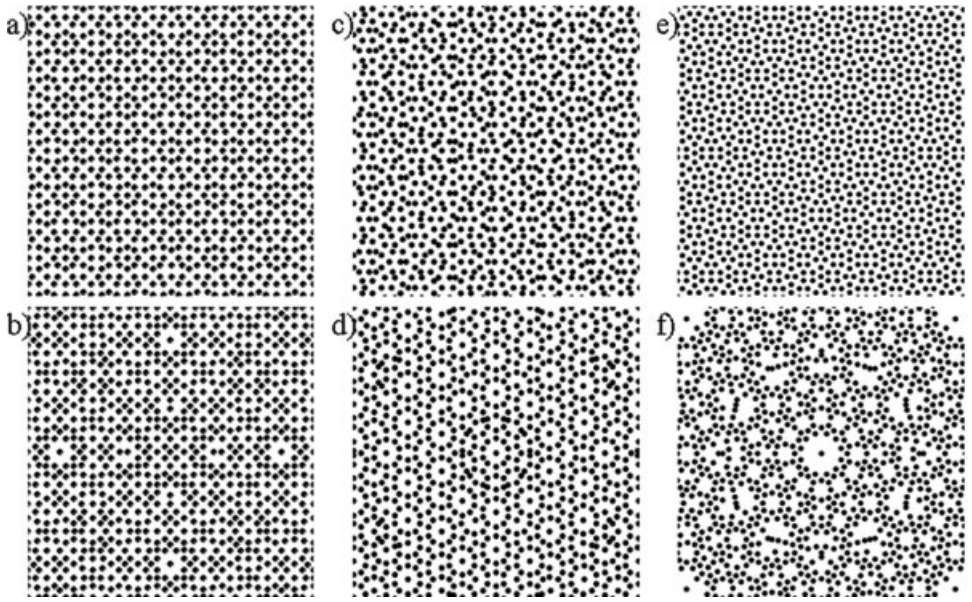

Figure 1 (a) and (b) Octagonal patterns of rods (top view) with geometric square-rhombus tiling (Ammann-Beenker) and interferential tiling, respectively; (c) and (d) decagonal patterns with geometric rhombic tiling (Penrose) and interferential tiling, respectively; (e) and (f) dodecagonal geometric triangle-square tiling (Stampfli inflation rule) and interferential tiling, respectively

the same linear polarization and equal optical phase, that is $\varphi_1 = \ldots = \varphi_8 = \ldots = \varphi_{12}$.

Because of the nongeometric building of the patterns depicted in Figures 1(b), 1(d), and 1(f), we found useful to define a new parameter, that is the average distance a between neighboring rods along the x-direction, as characteristic length of the patterns. This parameter was used to design the geometric patterns too. The filling factor is related to the ratio r/a, where r is the rod radius. Such parameter was held fixed to $r/a = 0.18$ in each simulation to permit the comparison between the structures analyzed here.

3. TRANSMISSION PROPERTIES OF QUASICRYSTAL STRUCTURES

As mentioned earlier, two different tiling patterns, obtained from geometric tiling and interference-based method, respectively, were analyzed for octagonal, decagonal, and dodecagonal symmetry.

The two-dimensional FDTD method with Perfectly Matched Layer boundary conditions (along x- and y-direction) was used in all simulations [20]. The FDTD technique was used to obtain transmission information, through the (x, y)-plane, as a function of propagation direction and wavelength, for both TE (electric field E_z perpendicular to the lattice plane) and TM (magnetic field H_z perpendicular to the lattice plane) polarization. In each numerical simulation, a Gaussian time-pulse excitation was launched from outside the structure or inside it for comparison. Several detectors (time monitors) were placed in specific positions allowing to store the field components in correspondence of a particular propagation direction of the light source [24]. Their positions were chosen to cover the angular range related to the 8-, 10-, and 12-fold rotational symmetry with an angular separation from 5 to 15° depending on the structure under study. The Fourier Transform of the time-dependent signal collected by the detector and normalized with respect to the incident light provided the frequency response of the structure with a high resolution. The corresponding transmission spectra had a wavelength range between 0.1 and 6.0 μm with a resolution of $\delta = 5.0 \times 10^{-4}\mu$m, whereas the discretization grid provided a minimum of 100 grid points per free space wavelength. The transmission coefficient was calculated as a function of the refractive index difference Δn for each propagation direction of the time-pulse source. The data collected from the detectors placed at different positions and angular orientations presented the same overall shape and band-gap properties, demonstrating that the structures are almost isotropic with respect to the propagation direction. The transmission spectra reported here were then obtained by taking the data collected from a single detector by fixing the incidence direction.

In Figure 2, the transmittance spectra related to the octagonal (A), left panel and octagonal (B), right panel patterns, obtained for increasing values of the refractive index difference Δn, in particular 0.4 (a) and (b), 0.6 (c) and (d), and 0.8 (e) and (f), are shown as a function of normalized wavelength λ/a, for both TE (black curve) and TM (red curve) polarization. In the case of the octagonal (A) tiling, the bandgap starts to appear even at $\Delta n = 0.4$ [see Fig. 2(a)], but for TE polarization only. As the dielectric contrast increases, the attenuation of the transmission signal in the bandgap region enhances from ~13 to 30dB [see Figs. 2(a) and 2(e)] with an increase of the width to midgap ratio $\Delta\lambda/\lambda_m$ from 2.4% at $\Delta n = 0.4$–14.4% at $\Delta n = 0.8$. The attenuation was estimated by averaging the values obtained in correspondence of the spectral gap. The shift in the position of the bandgap, evident from the variation of the normalized midgap wavelength λ_m/a from 1.22 to 1.38, is reasonable because increasing values of Δn correspond to an increase in the average refractive index of the quasicrystal medium. In the case of the octagonal (B) tiling, the bandgap starts to appear at $\Delta n = 0.6$, centered at $\lambda_m/a = 1.79$, once again for TE polarization only [Fig. 2(d)]. In Figure 2(f), two bandgaps are instead visible corresponding to $\Delta n = 0.8$. The first one is centered at the normalized wavelength $\lambda_m/a = 1.61$ and the other one at $\lambda_m/a = 1.93$. The first bandgap has $\Delta\lambda/\lambda_m = \sim 5\%$ and presents a substructure of peaks that might be related to the existence of localized states. Very interesting is the presence of strong transmittance attenuations, of the order of ~50dB and ~30dB, found in the gap regions at $\lambda_m/a = 1.61$ and $\lambda_m/a = 1.93$, respectively.

The same procedure was applied to derive the bandgap properties of the decagonal quasicrystalline structures. The correspond-

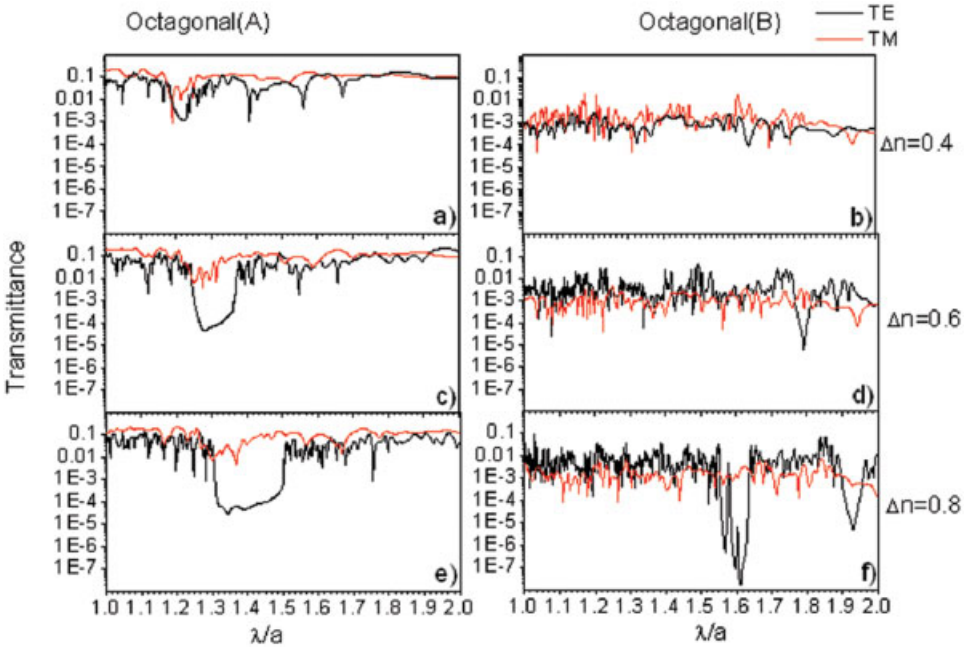

Figure 2 Transmittance spectra calculated for eightfold symmetry structures with geometric tiling, octagonal (A) (left panel), and interferential tiling, octagonal (B) (right panel), for TE (black curves) and TM (red curves) polarization, and increasing values of the refractive index difference: $\Delta n = 0.4$ (a) and (b), $\Delta n = 0.6$ (c) and (d), and $\Delta n = 0.8$ (e) and (f). [Color figure can be viewed in the online issue, which is available at www.interscience.wiley.com]

ing TE (black line) and TM (red line) transmittance spectra for both decagonal (A), left panel and decagonal (B), right panel patterns, obtained for $\Delta n = 0.4$ (a) and (b), 0.6 (c) and (d), and 0.8 (e) and (f) as a function of normalized wavelength λ/a, are presented in Figure 3. For TE polarization, the decagonal (A) pattern shows a tiny bandgap at a refractive index difference $\Delta n = 0.4$ with a ~5dB attenuation [see Fig. 3(a)], which enhances to ~20dB as the index difference increases to $\Delta n = 0.6$, with $\Delta\lambda/\lambda_m = 3.7\%$ at $\lambda_m/a = 1.45$ [see Fig. 3(c)]. The signal attenuation further increases to ~30dB with a normalized width $\Delta\lambda/\lambda_m = 9\%$ at $\lambda_m/a = 1.5$ for $\Delta n = 0.8$, as reported in Figure 3(e). No clear PBG was found for TM polarization, at least for the values of dielectric contrast examined here. As evident from the right panel of Figure 3, the decagonal (B) pattern, on the other hand, does not show any clear bandgap for both polarizations at $\Delta n = 0.4$ and 0.6 [see Figs. 3(b) and 3(d)]. For $\Delta n = 0.8$, a feature with ~20dB attenuation is

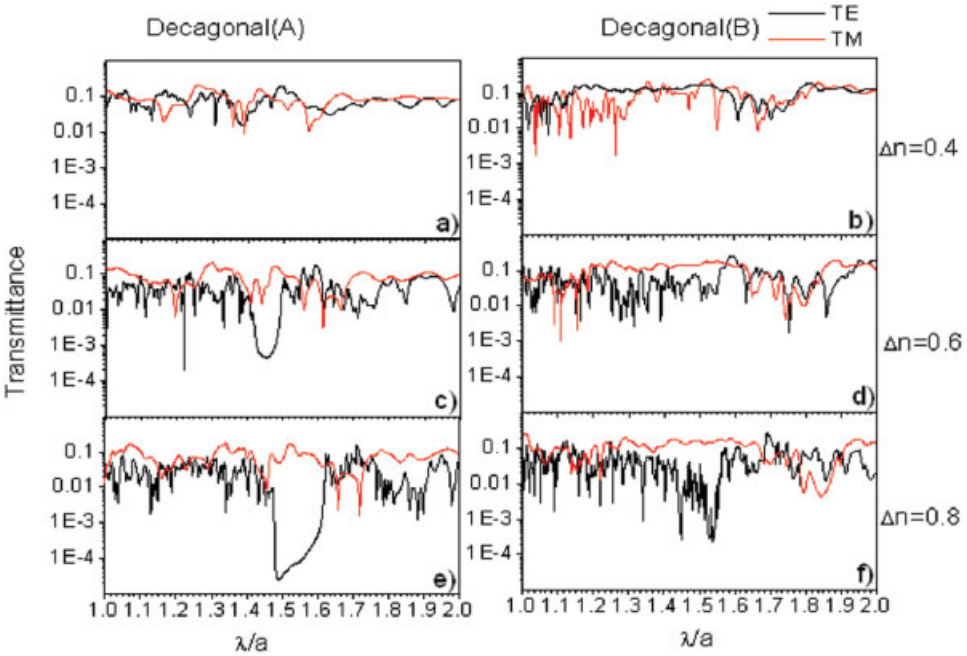

Figure 3 Transmittance spectra calculated for 10-fold symmetry structures with geometric tiling, decagonal (A) (left panel), and interferential tiling, decagonal (B) (right panel), for TE (black curves) and TM (red curves) polarization, and increasing values of the refractive index difference: $\Delta n = 0.4$ (a) and (b), $\Delta n = 0.6$ (c) and (d), and $\Delta n = 0.8$ (e) and (f). [Color figure can be viewed in the online issue, which is available at www.interscience.wiley.com]

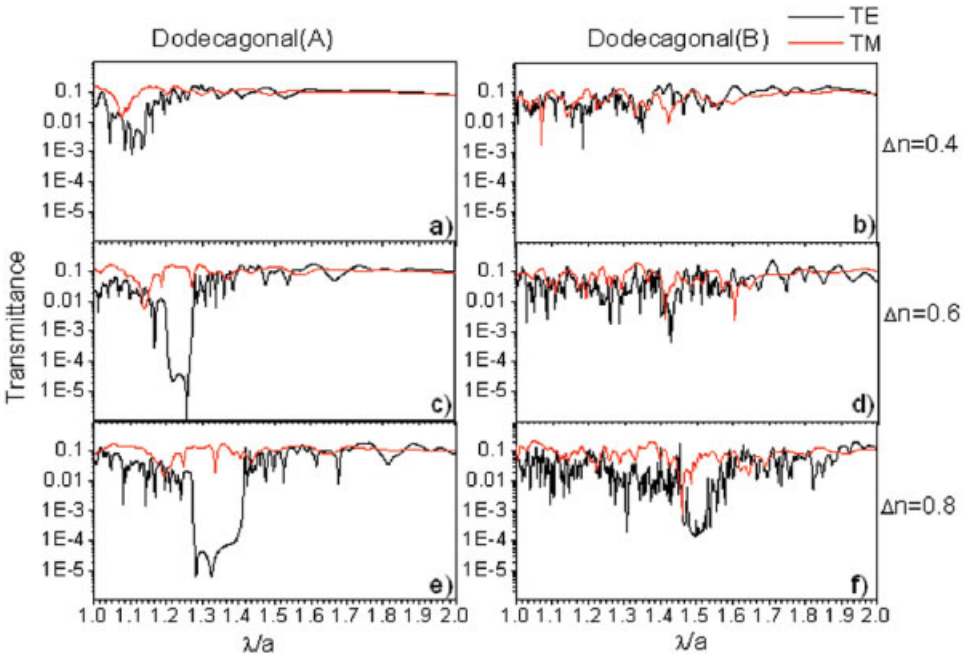

Figure 4 Transmittance spectra calculated for 12-fold symmetry structures with geometric tiling, dodecagonal (A) (left panel), and interferential tiling, dodecagonal (B) (right panel), for TE (black curves) and TM (red curves) polarization, and increasing values of the refractive index difference: $\Delta n = 0.4$ (a) and (b), $\Delta n = 0.6$ (c) and (d), and $\Delta n = 0.8$ (e) and (f). [Color figure can be viewed in the online issue, which is available at www.interscience.wiley.com]

visible in the transmission spectrum for TE polarization at $\lambda_m/a = \sim 1.5$ in a narrow range in which many other dips, associable to defect states, are present. This "bandgap" decreases even further for TM polarization ($\sim$10dB attenuation at $\lambda_m/a = \sim 1.8$), as shown in Figure 3(f).

The transmittance spectra associated to the 12-fold quasicrystals, dodecagonal (A) and (B), were calculated and reported in the left and right panels of Figure 4, respectively, analogously to the other structures previously analyzed. For the dodecagonal (A) tiling pattern, the bandgap starts to open up at $\Delta n = 0.4$ [Fig. 4(a)] for TE polarization, becoming wider at $\Delta n = 0.6$ with a normalized width $\Delta\lambda/\lambda_m = 5.7\%$ at $\lambda_m/a = 1.24$ and $\sim$25dB of attenuation in the transmission coefficient [see Fig. 4(c)]. The bandgap is shifted to $\lambda_m/a = 1.34$ with an increased width of $\Delta\lambda/\lambda_m = 10.3\%$ and an attenuation of $\sim$30dB at $\Delta n = 0.8$ [see Fig. 4(e)]. The interferential pattern [dodecagonal (B)] shows only a very narrow bandgap, for TE polarization and index difference as low as $\Delta n = 0.6$ in correspondence of the normalized midgap wavelength $\lambda_m/a = 1.43$. The bandgap width increases to $\Delta\lambda/\lambda_m = 4.5\%$, slightly shifted to $\lambda_m/a = 1.50$, at $\Delta n = 0.6$ and with an attenuation $<$20dB, although few localized states are visible within this spectral region, as reported in Figure 4(f). Also in this case, no remarkable photonic bandgap is observed in both (A) and (B) patterns for TM polarization of the time-pulse excitation.

From these simulations, it appears clear that the patterns under study—obtained from geometric algorithms or resulting from a multiple-beam holographic process—show remarkable differences not only with regard to the PBG properties but also in relation to the existence of the bandgap. The differences arisen from the transmittance spectra clearly point out the importance of the tiling geometry in determining the photonic bandgap properties of the quasicrystal, independently of the dielectric contrast and the rotational symmetry of the quasilattices studied in this work.

4. CONCLUSIONS

In this work, we analyzed the formation and development of the photonic bandgap in 2D 8-, 10-, and 12-fold symmetry quasicrystalline lattices of low-dielectric contrast. In particular, two different quasiperiodic patterns were considered and compared for each fixed order of symmetry. Our numerical simulations of the transmittance spectra, based on the finite difference method, prove that the different tiling geometry, more than the rotational symmetry, dramatically affects the existence and behavior of the photonic bandgap in low-dielectric contrast structures. If wide PBGs are to be obtained for small Δn, hence, very accurate control of the fabrication parameters is mandatory. The patterns that we examined here were chosen to highlight the substantial and remarkable PBG differences that arise between a quasicrystalline geometric tiling and a similar quasicrystal achievable from holographic fabrication techniques. Holographic lithography represents, in fact, an efficient and feasible fabrication method able to provide large-area PhQCs of high quality both in soft and hard materials [12–16]. In this direction, we have recently developed a single-beam holographic technique able to provide the desired tiling patterns to realize high-efficiency PBG structures for photonic applications [21, 22].

REFERENCES

1. D. Levine and P.J. Steinhardt, Quasicrystals: A new class of ordered structures, Phys Rev Lett 53 (1984), 2477–2480.
2. Z.M. Stadnik, Physical properties of quasicrystals, Springer, New York, NY, 1999.
3. Y.S. Chan, C.T. Chan, and Z.Y. Liu, Photonic band gaps in two-dimensional photonic quasicrystals, Phys Rev Lett 80 (1998), 956–959.
4. X. Zhang, Z.Q. Zhang, and C.T. Chan, Absolute photonic band gaps in 12-fold symmetric photonic quasicrystals, Phys Rev B 63 (2001), 0811051–0811054.

5. J.B. Suck, M. Schreiber, and P. Haussler, Quasicrystals, Springer, Berlin, 2002.
6. S.S.M. Cheng, L. Li, C.T. Chan, and Z.Q. Zhang, Defect and transmission properties of two-dimensional quasiperiodic photonic bandgap systems, Phys Rev B 59 (1999), 4091–4099.
7. C. Jin, B. Cheng, B. Man, Z. Li, D. Zhang, S. Ban, and B. Sun, Band gap and wave guiding effect in a quasiperiodic photonic crystal, Appl Phys Lett 75 (1999), 1848–1850.
8. M.E. Zoorob, M.D.B. Charlton, G.J. Parker, J.J. Baumberg, and M.C. Netti, Complete photonic bandgaps in 12-fold symmetric quasicrystals, Nature 13 (2000), 404.
9. C. Jin, B. Cheng, B. Man, Z. Li, and D. Zhang, Band gap and wave guiding effect in a quasiperiodic photonic crystal, Appl Phys Lett 75 (1999), 13–27.
10. E. Di Gennaro, S. Savo, A. Andreone, V. Galdi, G. Castaldi, V. Pierro, and M.R. Masullo, Mode confinement in photonic quasicrystal point-defect cavities for particle accelerators, Appl Phys Lett 93 (2008), 164102.
11. E. Di Gennaro, C. Miletto, S. Savo, A. Andreone, D. Morello, V. Galdi, G. Castaldi, and V. Pierro, Evidence of local effects in anomalous refraction and focusing properties of dodecagonal photonic quasicrystals, Phys Rev B 77 (2008), 193104.
12. X. Wang, C.Y. Ng, W.Y. Tam, C.T. Chan, and P. Sheng, Large-area two-dimensional mesoscale quasicrystals, Adv Mater 15 (2003), 1526–1528.
13. R.C. Gauthier and A. Ivanov, Production of quasicrystal template patterns using a dual beam multiple exposure technique, Opt Express 12 (2004), 990–1003.
14. X. Wang, J. Xu, J.C.W. Lee, Y.K. Pang, W.Y. Tam, C.T. Chan, and P. Sheng, Realization of optical periodic quasicrystals using holographic lithography, Appl Phys Lett 88 (2006), 0519011–0519013.
15. S.P. Gorkhali, J. Qi, and G.P. Crawford, Electrically switchable mesoscale Penrose quasicrystal structure, Appl Phys Lett 86 (2005), 0111101–0111103.
16. Y. Yang, S. Zhang, and G.P. Wang, Fabrication of two-dimensional metallodielectric quasicrystals by single-beam holography, Appl Phys Lett 88 (2006), 2511041–2511043.
17. S.P. Gorkhali, J. Qi, and G.P. Crawford, Switchable quasicrystal structures with five-, seven-, and ninefold symmetries, J Opt Soc Am B 23 (2006), 149–158.
18. G. Zhou and M. Gu, Photonic band gaps and planar cavity of two-dimensional eigthfold symmetric void-channel photonic quasicrystal, Appl Phys Lett 90 (2007), 2011111–2011113.
19. J.E.S. Socolar, Simple octagonal and dodecagonal quasicrystals, Phys Rev B 39 (1989), 10519–10551.
20. J. Romero-Vivas, D.N. Chigrin, A.V. Lavrinenko, and C.M. Sotomayor Torres, Resonant add-drop filter based on a photonic quasicrystal, Opt Express 13 (2005), 826–835.
21. G. Zito, B. Piccirillo, E. Santamato, A. Marino, V. Tkachenko, and G. Abbate, Two-dimensional photonic quasicrystals by single beam computer generated holography, Opt Express 16 (2008), 5164.
22. G. Zito, B. Piccirillo, E. Santamato, A. Marino, V. Tkachenko, and G. Abbate, FDTD analysis of photonic quasicrystals with different tiling geometries and fabrication by single-beam computer-generated holography, J Opt A: Pure Appl Opt 11 (2009), 0240071–0240078.
23. M. Bayindir, E. Cubukcu, I. Bulu, and E. Ozbay, Photonic band-gap effect, localization, and waveguiding in the two-dimensional Penrose lattice, Phys Rev B 63 (2001), 161104.
24. R.C. Gauthier and K. Mnaymneh, Photonic band gap properties of 12-fold quasi-crystal determined through FDTD analysis, Opt Express 13 (2005), 1985–1998.

PARAMETRIC STUDY OF GUIDED RESONANCES IN OCTAGONAL PHOTONIC QUASICRYSTALS

Ilaria Gallina,[1,2] Armando Ricciardi,[3] Marco Pisco,[4] Stefania Campopiano,[3] Giuseppe Castaldi,[1] Andrea Cusano,[4] Antonello Cutolo,[4] and Vincenzo Galdi[1]

[1] Waves Group, Department of Engineering, University of Sannio, Benevento, Italy; Corresponding author: vgaldi@unisannio.it

[2] Department of Environmental Engineering and Physics, University of Basilicata, Potenza, Italy

[3] Department for Technologies, University of Naples Parthenope, Naples, Italy

[4] Optoelectronic Division, Department of Engineering, University of Sannio, Benevento, Italy

Received 20 May 2009

ABSTRACT: *In this article, following up on our previous investigations on guided resonances (GRs) in photonic quasicrystal slabs based on octagonal (quasiperiodic) tilings, we present the salient results from a parametric study of the GR properties, varying the air/dielectric fraction, and the slab refractive index and thickness. Our results, obtained via full-wave simulations, show similar qualitative trends as those observed in the literature for periodic photonic crystal slabs.* © 2009 Wiley Periodicals, Inc. Microwave Opt Technol Lett 51: 2737–2740, 2009; Published online in Wiley InterScience (www.interscience.wiley.com). DOI 10.1002/mop.24721

Key words: *photonic quasicrystals; guided resonances; periodic photonic slabs*

1. INTRODUCTION

Recently, a large body of studies have been devoted to the defect and bandgap engineering of photonic crystal (PC) slabs, mainly aimed at designing micro- and nano-sized optical devices for integrated photonic circuits (see, e.g., [1–7] for a sparse sampling).

In most applications of interest, PC slabs made of air hole arrays in a host dielectric medium typically support "guided modes," which, in a band diagram, are represented below the light line; these modes are completely confined within the slab (because of total internal reflection [8, 9]), and unable to couple to any external radiation. However, PC slabs can also support the so-called "*leaky* modes," represented, in a band diagram, above the light line, and characterized by finite lifetimes, electromagnetic (EM) power strongly confined within the slab, and yet the ability to couple to the continuum of free-space modes; for this reason, these modes are known as "guided resonances" (GRs) [10]. Illuminating the PC slab with a normally incident (with respect to the plane of crystal periodicity) plane wave, the interference between the directly transmitted/reflected wave and the waves originating from the excited GRs can generate in the transmittance/reflectance spectra narrow Fano-like resonant line shapes [11, 12] (whose center frequencies and linewidths depend on the geometric and physical parameters of the PC structure, as well as on the direction and polarization of the incident wave [13]) superimposed on a smoothly varying background resulting from the Fabry-Perot effect associated to the light interaction with an effectively-homogeneous dielectric slab. The reader is referred to [14–21] (and the references therein) for a sparse sampling of recent studies addressing the properties and potential applications of GRs.

In a series of ongoing investigations [22], we have been concerned with the study of GRs in aperiodically-ordered "photonic quasicrystal" (PQC) [23] slabs, intrinsically tied to the concept of "quasicrystal" in solid-state physics [24]. We showed that, in spite of the seemingly necessary spatial periodicity [21], GRs could also